Astrophys Space Sci (2009) 323: 357–366
DOI 10.1007/s10509-009-0079-6

ORIGINAL ARTICLE

# A Moon-borne electromagnetic calorimeter

**Roberto Battiston · Maria Teresa Brunetti · Franco Cervelli · Cristiano Fidani · Mauro Menichelli**

Received: 27 February 2009 / Accepted: 29 July 2009 / Published online: 22 August 2009


**Abstract** We discuss an electromagnetic sampling calorimeter for the detection of very high energy gamma-rays on the Moon, which is based on the use of scintillating cylinders and plates imbedded in the lunar soil. The use of lunar soil as a calorimeter radiator reduces the weight of the material to be transported to the Moon and minimises environmental impact. Plastic scintillator bars inserted into the regolith about 1.5 m are the active elements of this instrument: at the surface, each bar is terminated by a plastic scintillator plate to veto high energy charge particles. The readout system for the scintillator bars and plates are based on recently developed single photon solid state detectors (Silicon Photomultiplier, SiPM), extremely compact, sturdy and sensitive devices suited for detecting small light pulses in a space experiment. The performance of a regolith-scintillator calorimeter is evaluated and the relevant parameters are optimised using a GEANT4 simulation.

**Keywords** Gamma-ray · Semiconductor light detector · Lunar regolith · Monte Carlo · GEANT4

R. Battiston · M.T. Brunetti · C. Fidani (✉) · M. Menichelli
Istituto Nazionale di Fisica Nucleare—Sezione di Perugia, Perugia, Italy
e-mail: cristiano.fidani@fisica.unipg.it

R. Battiston
Dipartimento di Fisica, Universitá degli Studi di Perugia, Perugia, Italy

F. Cervelli
Istituto Nazionale di Fisica Nucleare—Sezione di Pisa, Pisa, Italy

## 1 Introduction

The renewed interest in planetary exploration following the plans issued by the NASA administration in 2005 (Griffin 2005) calls for new ideas regarding science experiments to be performed on the Moon. It is a common opinion that the Moon environment is particularly suitable for the study of space phenomena which are not accessible from the Earth as it is screened by the atmosphere (Spudis 2001). This is particularly true for the study of high energy charged particles and gamma-rays coming from space; here the presence of the atmosphere forbid the detection of the primary particles reaching the Earth (Foing 1996).

In this study we analysed to what extent a moon-based instrument could be competitive for the study of the energetic electromagnetic component of cosmic radiation in the energy range from 10 GeV to few TeV and greater. The exploration of this part of the electromagnetic spectrum from space is very difficult because of the weights and sizes of the required instruments. The FERMI—Gamma-ray Large Area Space Telescope, launched on June 11, 2008, is the most sensitive high energy gamma-ray space instrument ever launched; it will cover the energy spectrum for up to about 300 GeV (Tajima 2006). On the other side, the recent progress of Cerenkov telescopes (Hinton and Egberts 2008) makes possible the study of sources of gamma-rays in the same region (i.e. starting from ∼30 GeV), but with an energy resolution never better than 15–20% from Earth and it will not allow to study the diffuse emission of energetic gamma-rays due to the large background induced by charged cosmic rays (CR).

A moon-based electromagnetic calorimeter could largely extend the acceptance with respect to both space based and ground based gamma-rays detectors. Furthermore an imaging calorimeter could also provides the direction of the in-

coming gammas, so contributing to discriminate between galactic and extragalactic sources. The design of this kind of detector should fulfill three requirements. The first, regards the converter: we propose using the lunar soil, the regolith, to minimise the upmass needed to build a calorimeter. The second, concerns the detecting element: it must be simple and easy to assemble, so to enable fully automatic missions. The third, regarding the modularity of the detector which can be built as the sum of $n$-independent modules and can be added to the existing sample without limitations. This last feature would allow the detector to be operative already after its first installation on the Moon. The initial detector could indeed be expanded during following missions by adding more and more modules.

These three requirements have been implemented in the design of a new kind of "Spaghetti" calorimeter (Spacal) (De Salvo 1995), described in this paper herein after as "Moon" calorimeter (Mooncal). On the Mooncal the lunar regolith is the radiator for producing the electromagnetic (EM) showers: the EM showers are then sampled by longitudinally segmented plastic scintillator cylinders, embedded in aluminum cylinders vertically inserted into the lunar regolith. The incoming charged particles can be selected by the use of thin scintillator plates on the top of each cylinder, which will act as veto counters, and by the energy distribution pattern.

## 2 Studying gamma and electron fluxes on the Moon surface

The gamma observation is aimed at the identification of different galactic sources (Greiner 2007) such as: diffused components (Strong 2007), supernova remnants (Funk 2008), pulsar wind nebulas (Aharonian et al. 2006), gamma-ray binaries (Dubus 2008), molecular clouds (Aharonian et al. 2008a), clusters of massive stars (Aharonian et al. 2007). Also extra-galactic sources can be studied (Beilick 2007) such as: diffused components (Pavlidou et al. 2008), active galactic nuclei (Aharonian et al. 2008b) and gamma-ray bursts (Fan and Piran 2008). Several unidentified sources have also been recorded (Funk 2007; Aharonian et al. 2008c). To date, the detection and subsequent study of all the known TeV gamma sources have been made by means of ground-based Imaging Atmospheric Cherenkov Telescope (IACT) systems such as the High Energy Stereoscopic System (HESS) and the Major Atmospheric Gamma-Ray Imaging Cherenkov Observatory (MAGIC). Mooncal may extend the physics reach of these observatories because the absence of atmosphere virtually eliminates the background induced by charged CR making the measurement of extended sources possible.

Improvements could be expected also in the measurement of electron sources in the TeV region such as Vela, Cygnus loop and Monogem (Kobayashi et al. 2004). It is also expected that annihilations of dark matter particles could create detectable features on the positrons and electron spectra in the O(100) GeV region. Here we refer to predictions based on the existence of neutralino particles from SUSY or Kaluza-Klein theories (Bertone et al. 2005). Although Mooncal cannot distinguish positive charges from negative ones, such an excess of positrons and electrons could be detected thanks to the excellent energy resolution as well to the large statistics which could be accumulated.

The Mooncal energy resolution improves at higher energy: consequently it should be able to precisely measure features in the gamma-rays spectrum such as those predicted by the annihilation of SUSY particles (Kuhlen et al. 2008). Moreover, Mooncal will be able to carry out observations above several hundreds of GeV (Tajima 2006), extending the energy reach of FERMI. In addition, Mooncal combines the large field of view of space detectors, with a much larger collecting area than FERMI, which makes it well suited for the observations of long-term behavior of several sources.

**Table 1** Regolith chemical composition from the Apollo missions

| Chemical composition | In % mass |
|---|---|
| $SiO_2$ | 42.1 |
| FeO | 17.4 |
| $Al_2O_3$ | 13.0 |
| CaO | 11.3 |
| MgO | 8.0 |
| $TiO_2$ | 7.2 |
| $Cr_2O_3$ | 0.27 |
| MnO | 0.20 |
| Na | 3150 (ppm) |
| K | 1090 (ppm) |

## 3 Characteristics of Moon soil

The surface of the Moon is almost completely covered by a layer of soft powder, called lunar regolith, which is the result of continuous meteoroid impacts on the lunar bedrock. Table 1 shows the regolith chemical composition in percentage mass as was taken by the measurements of the American Apollo missions (Heiken et al. 1991). The depth of this layer varies from 4–5 m in the lunar maria (main craters) to about 10–15 m elsewhere. The density of the regolith was evaluated thanks to deep core samples of lunar soil collected during the Apollo missions; its extrapolated function is shown in Fig. 1 (Heiken et al. 1991). A more detailed lunar map of thickness has been evaluated by using radar and optical data (Shkuratov and Bondarnko 2001, 2002; Champbell 2002), and it is in agreement with previous results. The

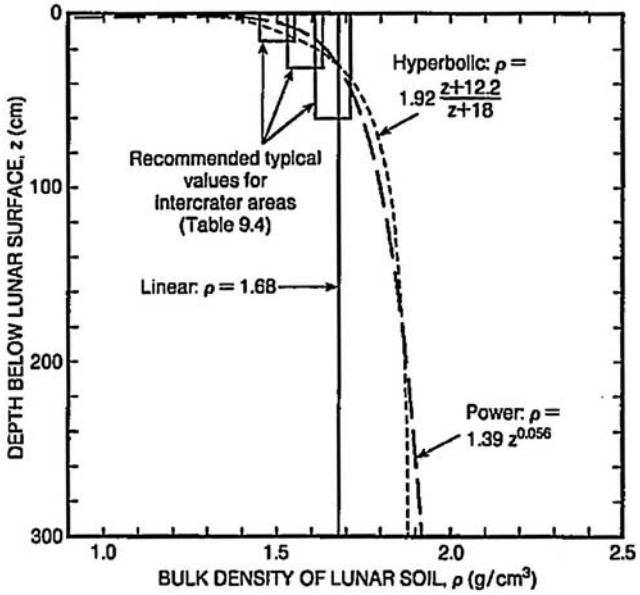


**Fig. 1** In situ bulk density of the lunar soil layer calculated as a function of depth below the surface. Three calculated density-depth relations are shown: linear (*solid line*), power-law (*heavily dashed line*), and hyperbolic (*lightly dashed line*). *Boxes* at the *top* of the plot show recommended near-surface bulk density values for out of crater areas, from Heiken et al. (1991)

measurements show that the regolith density in the surface of the Moon varies increasingly with depth, but it quickly approaches a maximum, and below a depth of about 50 cm it increases but more slowly. The surface density is about 1.2 g cm$^{-3}$ while a substratum density of 3.2 g cm$^{-3}$ for the maria regions and 2.9 g cm$^{-3}$ for other regions have been reported (Heiken et al. 1991).

The common type of particles found in the lunar regolith can be classified as follows: unshocked and shocked crystalline rock fragments and mineral grains, regularly shaped glass (including spherical shapes, dumbells and tear drops), glass fragments of irregular shape, agglutinates (glass bonded aggregates of grains) and microbreccia fragments (King 1977). The mean size of regolith particles is about 0.1 mm (Heiken et al. 1991).

The uppermost layer of the regolith rises and falls easily due to the reduced gravitational force and the presence of electrostatic interactions. This phenomenon has been observed in the lunar horizon at sunrise and sunset since the Apollo missions (Heiken et al. 1991). The Moon is therefore a dusty environment and this fact must be taken into account, especially when planning operations involving the use of regolith. During the operation of a Moon Base, several experiments and various activities will be carried out simultaneously. The sensitivity to massive dust rising could be a problem for some of the planned activities, which is avoided by the proposed technique here.

The variations in the solar radiation during the day-night cycle produce a corresponding variation in the surface temperature of the Moon. For the same reason, there is also a latitude dependency. Quite surprisingly, at a depth of 40 cm in the regolith, the temperature is almost stable at around −20°C (±3°C, in loco measurements) (Heiken et al. 1991). Figure 2 shows the temperature values as a function of the depth. Operating in a stable thermal environment is another advantage of the Mooncal approach.

## 4 Mooncal layout

The first applications of EM Spacal made of lead with fibers was in early 80' at CERN (Perrin and Sonderegger 1981). Mooncal geometry is simple and similar to Spacal, see Fig. 3: a flat circular area on the lunar surface with a radius of several meters is filled with scintillator bars inserted vertically into the regolith. The bars are positioned in a planar square grid pattern distanced a few centimeters apart from each other. Various parameters are varied in the simulations to obtain the best compromise between the detector performance and its feasibility. A scintillator depth from 150 cm to 300 cm is used, while the inter grid step is varied from 4 cm up to 15 cm and the scintillator radius between 0.5 and 1.0 cm.

The technical feasibility of the regolith-scintillator calorimeter is based upon the direct experience of the astronauts who repeatedly manually drilled without particular difficulties the lunar surface to sample the regolith down to a depth of 3 meters (Heiken et al. 1991). The required forces for excavation and traction were recently calculated for lunar regolith and improvements in terra-mechanics processing with robotic lunar missions were recommended (Wilkinson and DeGennaro 2007). Novel drilling techniques were proposed for thermal sensors in lunar and planetary regolith (Komle et al. 2008). In the present project, the idea is to use a robot to drill the regolith layer with an empty carbon fiber cylinder down to the depth corresponding to the scintillator bar length. The scintillator, equipped with its electronics readout, should then be placed in its proper location after the extraction of the regolith carrot.

Figure 4 shows a picture of the scintillator bar layout. As the value of the scintillator density is about 1 g cm$^{-3}$, the weight of a 150 cm long bar ranges from about 0.15 kg ($r = 0.5$ cm) to about 0.5 kg ($r = 1.0$ cm). The Mooncal could operate already after the first mission, with only a few hundred active elements buried in to the regolith. Thanks to the modularity of the detector subunits, it would then be possible to build a large acceptance calorimeter in successive steps.

Each Mooncal bar, see Fig. 4, consists of a cylindrical aluminium tube typically 0.5 to 1.0 cm in radius and 150

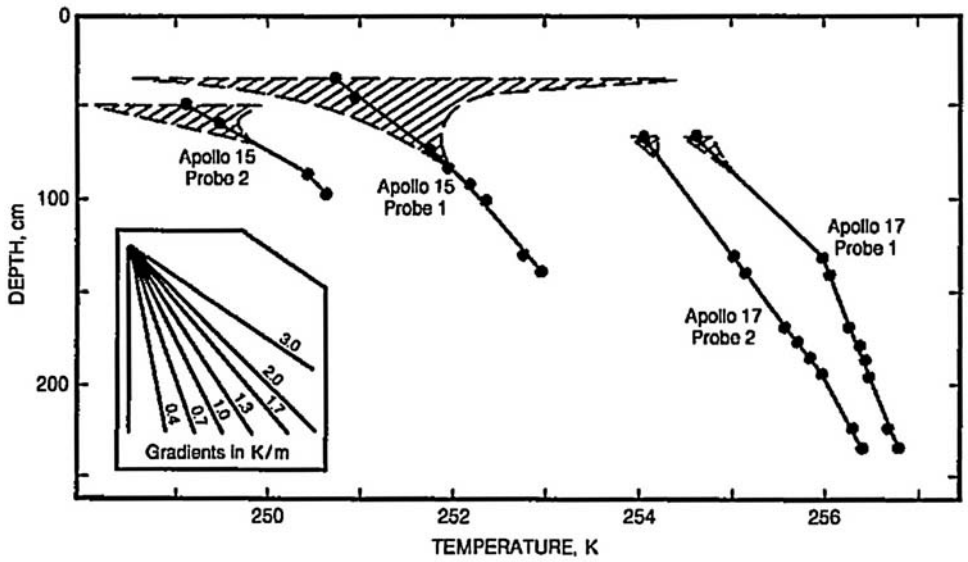


**Fig. 2** Observed temperature fluctuations in the lunar regolith as a function of the depth. The *dashed area* shows the day-night temperature fluctuations between 30 and 70 cm. The variations related to the solar radiation do not affect the temperature below a depth of 50 cm, from Heiken et al. (1991)

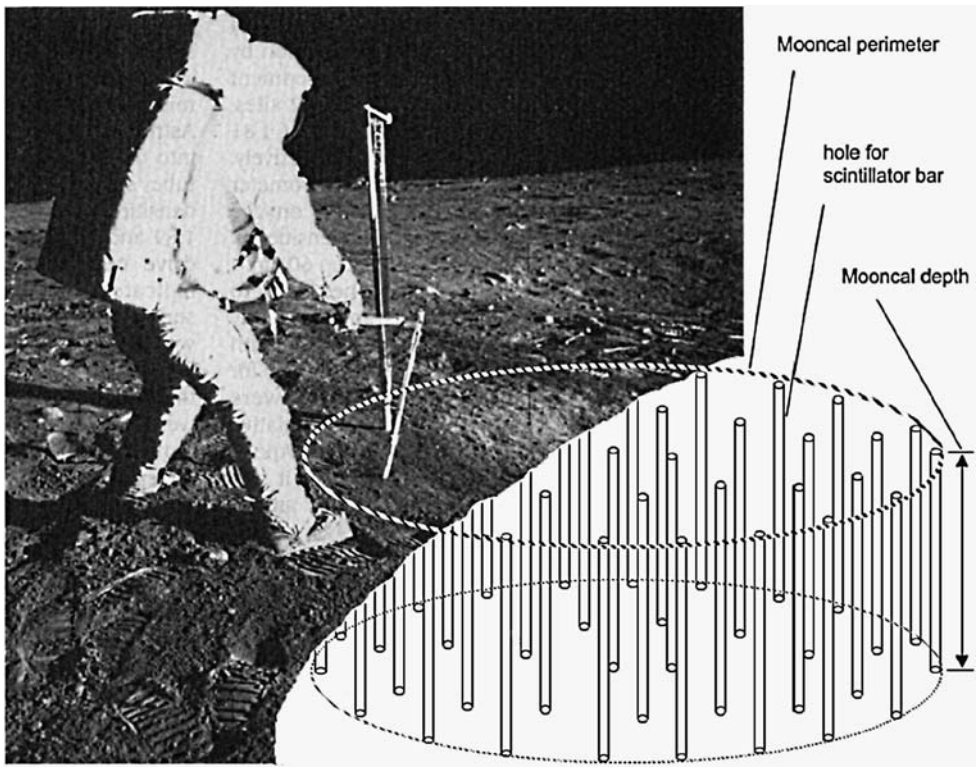


**Fig. 3** Astronaut Edwin Aldrin driving the core tube sampler into the lunar surface at the Apollo 11 landing site (Tranquillity Base), from Heiken et al. (1991). The hole cylinders were included in the photo to describe the geometry of Mooncal

to 300 cm long. These aluminum cases contain a stack of 15–30 scintillating bars elements, 0.45 to 0.95 cm in diameter. The longitudinal segmentation of each bar allows a three dimensional reconstruction of the EM shower. This imaging capability of the proposed calorimeter permits either the discrimination between the EM showers and hadronic cascades, either the determination of the gamma redirection (provided by the shower axis). Each of these is read by a Silicon Photo Multiplier (SiPM), a compact solid state single photon detector, located at the end of each element. Figure 4 shows the section view of a bar. The performance of the coupling between the SiPM and the scintillating bars is presently under study (Achenbach et al. 2008).

Details of the SiPM operational characteristics can be found in literature (Dinu et al. 2007). These devices typically have an operational voltage, as low as 30 V. The gain ranges from $10^5$–$10^6$. In order to exploit their properties it is necessary to operate the SiPMs at a constant temperature.

The Mooncal bars are completely inserted into the lunar regolith and they are equipped with a veto counter on

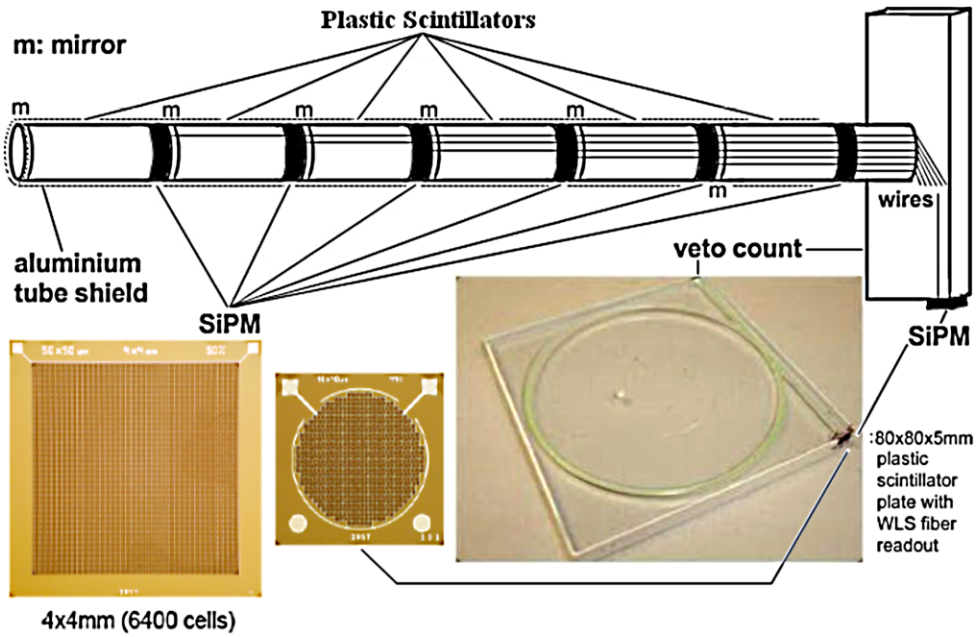


**Fig. 4** A sketch of a short scintillator bar. Photons produced in the plastic scintillator cylinders are read by SiPMs and reflected by mirrors. A veto counter on the top of the cylinder can also be realised with a rectangular plastic scintillator

**Table 2** Regolith elemental composition. MF: mass fraction; Ab: abundance

| Element | A($\frac{g}{mole}$) | MF(%) | Ab(%) |
|---|---|---|---|
| Oxygen | 16.00 | 42.26 | 60.32 |
| Silicon | 28.09 | 20.47 | 16.64 |
| Iron | 55.84 | 12.90 | 5.28 |
| Calcium | 40.08 | 8.15 | 4.64 |
| Aluminium | 26.98 | 6.99 | 5.91 |
| Magnesium | 24.30 | 5.61 | 5.27 |
| Titanium | 47.87 | 2.58 | 1.23 |
| Sodium | 22.99 | 0.30 | 0.29 |
| Chromium | 51.00 | 0.24 | 0.11 |
| Manganese | 54.94 | 0.17 | 0.07 |
| Potassium | 39.10 | 0.14 | 0.08 |
| Sulphur | 32.06 | 0.11 | 0.08 |
| Phosphorus | 30.97 | 0.09 | 0.07 |

their tops. The Mooncal veto is designed to reject the background of charged cosmic ray particles which is $10^3$–$10^4$ more intense, using a technique similar to the one used by the FERMI detector (Moiseev 2008).

## 5 The simulation of Mooncal

The Monte Carlo toolkit GEANT4 (Agostinelli et al. 2003) developed at CERN, Geneva, was used to simulate the response of the regolith-scintillator calorimeter. The elemental composition of the regolith and its density, were taken from the measurements of the American Apollo missions and Soviet Luna missions (Heiken et al. 1991). The mean values of the chemical components were calculated from the samples collected in the lunar maria and are reported in Table 2. Compared to the highland sites, the lunar maria sites are rich in iron and titanium, while poor in aluminum. A conservative number of 1.5 g cm$^{-3}$ was taken as the regolith density. With these settings, the regolith radiation length $X_0$ was calculated to be about 15 cm.

In Fig. 5, the parameter $r$ represents the radius of the scintillator bars; the values used in the Monte Carlo simulations were $r = 0.5$ cm and $r = 1$ cm. Because we wanted to design a calorimeter with a good energy resolution we tested four values for the distance d among the bars: $d = 4$ cm, 7.5 cm, 10 cm and 15 cm. We used two lengths of the bars $L = 150$ cm and $L = 300$ cm. The area covered in the simulation was a cylinder having a radius of 300 cm. According to these parameters, the number of simulated scintillator bars varied from 5,000 to about 17,700.

EM showers having incident angle between 45° and 80° with respect to the zenith are longitudinally contained in Mooncal. In order to assure lateral containment of the showers, the incident point of the incoming particle was taken within 1 meter from the calorimeter center.

Primaries in the energy interval between 100 MeV and 100 GeV were simulated using a Monte Carlo code. Here we concentrated on photons primaries because the resolution is worse with respect to electrons (Wigmans and Zeyrek 2002). The number of incident particles was always equal to 10,000. Figure 6 shows samples of the shower simulation: the grey cylinder represents the portion of Moon surface equipped with scintillator bars; EM showers induced by 10 GeV gamma-rays are shown, green lines = electrons, red lines = positrons while photons are omitted. Figure 7 de-

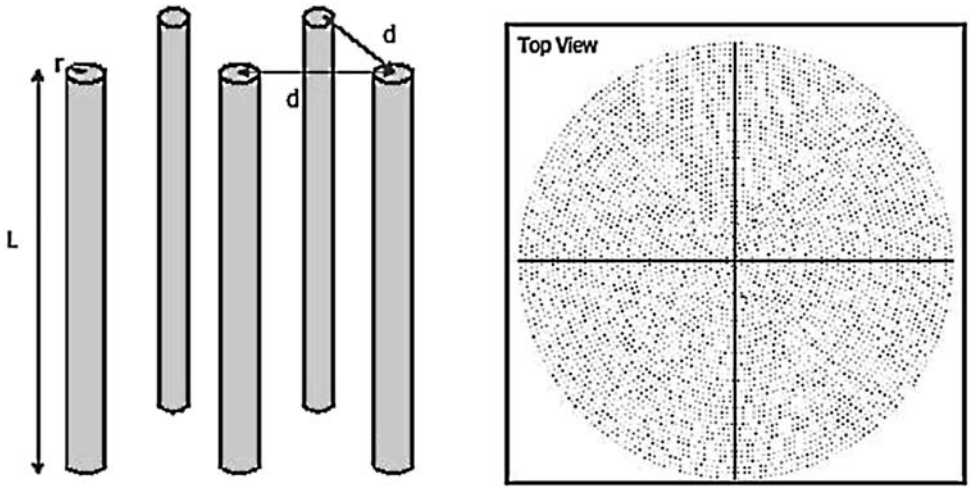


**Fig. 5** Layout of the scintillator bars to be vertically inserted into the lunar regolith. $L$ is the bar length, $r$ the radius and $d$ the distance among the bars

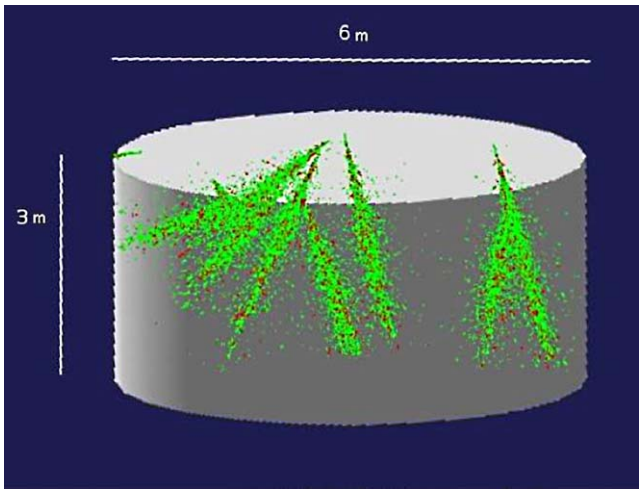


**Fig. 6** Electromagnetic showers induced by 10 GeV gamma-rays in the Mooncal (regolith-scintillator calorimeter). The electronic component is shown in *green* while positrons are in *red*. For the sake of clarity, the scintillator bars are not shown

**Table 3** Resolution fits of Fig. 8 where $r = 1$ cm; $*$ is calculated using $E = 100$ GeV

| $L$ (m) | $d$ (cm) | $a$ (%) | $b$ (%) | $c$ (%) | $\frac{\Delta E}{E}^*$ |
|---|---|---|---|---|---|
| 1.5 | 15.0 | $33.5 \pm 0.7$ | $42.6 \pm 3.7$ | $7.7 \pm 3.2$ | 0.378 |
| 1.5 | 10.0 | $19.6 \pm 0.7$ | $25.4 \pm 3.7$ | $7.2 \pm 3.1$ | 0.222 |
| 1.5 | 7.5 | $13.9 \pm 0.6$ | $14.1 \pm 3.4$ | $9.3 \pm 2.9$ | 0.154 |
| 3.0 | 7.5 | $11.6 \pm 0.4$ | $21.6 \pm 2.1$ | $3.6 \pm 1.8$ | 0.138 |

**Table 4** Resolution fits of Fig. 9 where $r = 0.5$ cm; $*$ is calculated for $E = 100$ GeV; $+$ Mooncal radii is increased to 10.0 m

| $L$ (m) | $d$ (cm) | $a$ (%) | $b$ (%) | $c$ (%) | $\frac{\Delta E}{E}^*$ |
|---|---|---|---|---|---|
| 3.0 | 7.5 | $14.1 \pm 0.7$ | $31.6 \pm 3.7$ | $7.3 \pm 3.1$ | 0.173 |
| 1.5 | 4.0 | $8.2 \pm 0.5$ | $6.6 \pm 2.5$ | $10.1 \pm 2.1$ | 0.09 |
| 3.0 | 4.0 | $5.7 \pm 0.4$ | $14.4 \pm 1.9$ | $5.2 \pm 1.7$ | 0.072 |
| $10.0^+$ | 4.0 | $4.7 \pm 0.3$ | $18.4 \pm 1.8$ | $2.1 \pm 1.5$ | 0.066 |

scribes axial and lateral sections view of the Mooncal simulation, together with a 100 GeV gamma-ray shower.

The energy resolution for a sampling calorimeter like Mooncal is represented by the relationship:

$$\frac{\Delta E}{E} = a \oplus \frac{b}{\sqrt{E}} \oplus \frac{c}{E}$$

where $E$ is the sampled energy in GeV, $\oplus$ indicates that the terms are added in quadrature, $\Delta E$ is the uncertainty, $a$, $b$ and $c$ are three constants, where $c$ describes the noise, $b$ describes the behavior at low energy while $a$ describes the high energy resolution limit. As the incident energy increases, the energy resolution decreases reaching a systematic limit at a very high energy.

Several simulations were performed with respect to different parameters, Fig. 8 shows the simulated energy resolution as a function of the incident gamma-ray energy with the following parameters: $r = 1$ cm, $L = 150$ and 300 cm and several $d$. The fits were performed with $d = 7.5$, 10 and 15 cm and the results are shown in Table 3. The dependency of the energy resolution on the distance $d$ among the scintillator bars can be appraised from Fig. 8. As expected, the energy resolution worsens as the granularity of the detector decreases. The highest energy resolution in Fig. 8 was obtained using $d = X_0/2$. This was about 12% in the high energy limit. However, in the case of a 7.5 cm distance between the active bars, the loss of containment increases the uncertainty in energy resolution, and longer active bars should be used; see last line in Table 3.

A better result can be reached with a shorter inter-bar distance corresponding to $d = 4$ cm, eve if a smallest radii ($r = 0.5$ cm) is used; see Fig. 9. The fits obtained in this case are shown in Table 4. A comparison between the continuous fit in Fig. 8 and the dashed-dotted fit in Fig. 9 shows that the

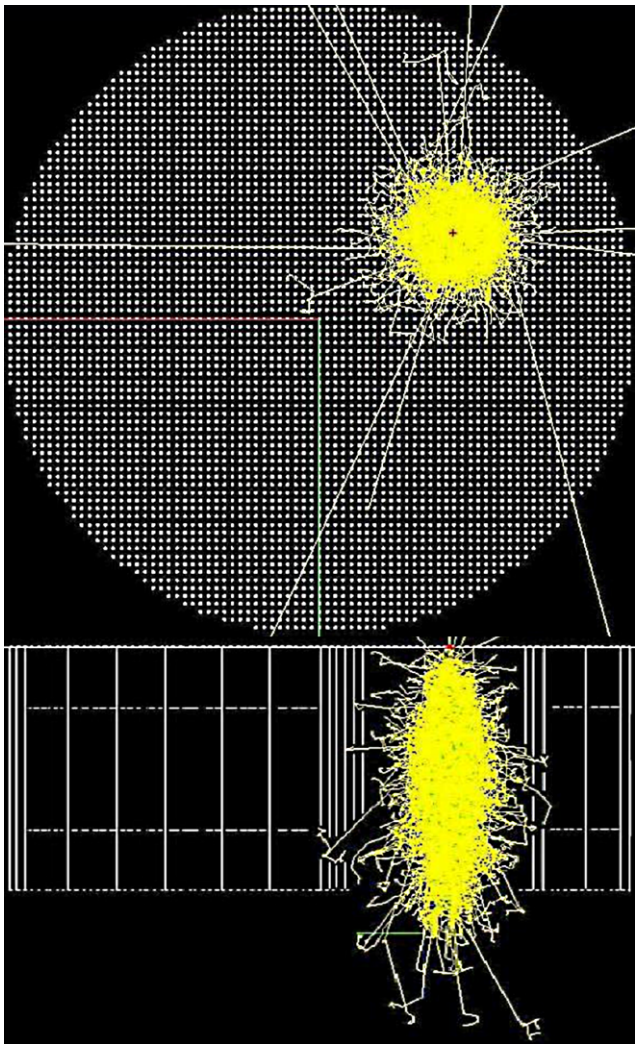

**Fig. 7** Photon showers induced by 100 GeV gamma-rays in two sections of the Mooncal. Photons are shown in *yellow*, electrons are in *green* and incident position in *red*

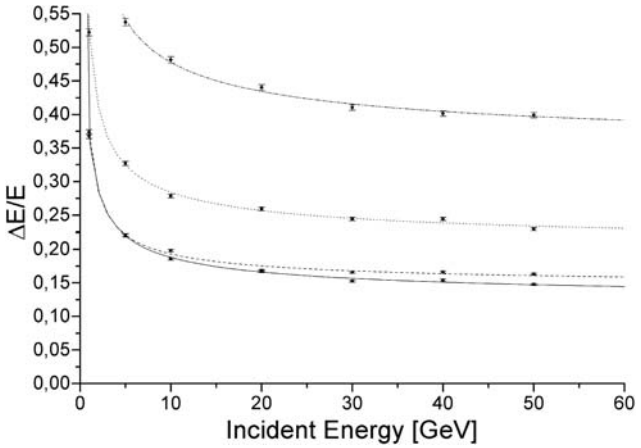


**Fig. 8** Energy resolution as a function of the photon energy incidence in the calorimeter. Mooncal parameters are: $r = 1$ cm, $L = 300$ cm and $d = 7.5$ cm (*continuous line*), $L = 150$ cm and $d = 7.5$ cm (*dashed line*), $L = 150$ cm and $d = 10$ cm (*dotted line*) and $d = 15$ cm (*dashed-dotted line*)

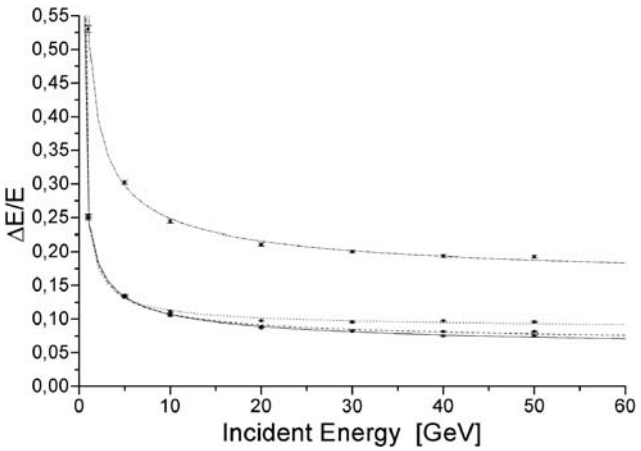


**Fig. 9** Energy resolution for the parameters $r = 0.5$ cm, $L = 150$ cm and $d = 4$ cm (*dotted line*), $L = 300$ cm and $d = 4$ cm (*dashed line*), $L = 1000$ cm and $d = 4$ cm (*continuous line*) and $L = 300$ cm and $d = 7.5$ cm (*dashed-dotted line*)

parameter $r$ plays an important role in determining the energy resolution; the resolution worsens with less scintillator volume and the same inter-bar distance $d$. Dashed, dotted and continuous fits in Fig. 9 shows that $d$ can be reduced to recover the lost resolution. Despite a reduction in the scintillator volume density of 0.88, obtained with $d = 4$ cm and $r = 0.5$ cm instead of $d = 7.5$ cm and $r = 1$ cm, a better resolution, due to a more regular scintillator distribution, was obtained. The best energy resolution was under 5% for the high energy limit. On the other hand, the noise term maintains the same value when reducing $d < X_0/2$ and $r < 1$ cm whatever the Mooncal depth. The continuous line in Fig. 9 was obtained with $L = 1000$ cm and this indicates the resolution limit of Mooncal when the showers are completely contained. Finally, the $b$ factor describes the behavior of Mooncal energy resolution in the low energy range, for example, the dotted fit of Fig. 9 shows a near constant energy resolution for $E > 10$ GeV, which corresponds to a small value of $b$.

The increased resolution with a smaller inter-bar distance will have a practical limit regarding soil insertion because of the smaller scintillator radius required. This limit will be important for the Mooncal weight which is a crucial point in every Moon based experiment. Therefore, the best compromise would be by following these parameters: $d = 4$ cm, $r = 0.5$ cm and $L = 150$ cm covering a 100 cm radius portion (a 3.14 m$^2$ area) of the Moon surface. This would correspond to about 2000 scintillator bars for a total weight of less than 300 kg, less then 4% of the Mooncal weight and about 5% of the Mooncal volume. The result of a simulation using this geometry is shown with the dotted line in Fig. 9,

where the energy resolution reaches a high energy limit of about 8%.

Geometry of Mooncal produces different instrumental responses depending on the direction of the incident cosmic-ray. The plot of the resolutions versus incident angles with respect to the zenith at different energies are shown in Fig. 10, when the Mooncal radius is 300 cm. Due to the shower length, compared to the Mooncal depth, the perpendicular cosmic-ray direction measurements are worse. In fact, we can observe a worsening resolution for higher energy (continuous line) and smaller angles. The minimum resolution, observed near 65° reflects the maximum diagonal length of Mooncal. At lower energy such an effect reduces (see dashed line) while resolution granularity phenomena appears to be due to the inter-bar distance using 5 GeV photons (dotted line). To have a precise idea of the detector containment, we have shown the fraction energy collected in Mooncal as a function of different photon energy incident angles in Fig. 11.

When the incident energy increases beyond 100 GeV the shower is no longer contained in this calorimeter. In this case, it is necessary that the energy to be estimated. A possible method for evaluating the high energy tails, is to perform a constrained fit of the Gamma distribution (Gavler et al. 2006)

$$\frac{dE}{dx} = E_o A \frac{(xA)^{B-1} e^{-xA}}{\Gamma(B)},$$

where $E_o$ is the incident energy, $x$ is the depth in radiation lengths, $A$ and $B$ are energy dependent parameters and $\Gamma$ is the Gamma function. For example, we calculated the energy deposition on 5 cm slabs of plastic scintillating cylinders (total length 150 cm or 30 slabs). The simulations were performed with 10 GeV incident gamma-rays using the parameters $d = 4$ cm, $r = 0.5$ cm and $L = 150$ cm. The energy distribution resulting from a 10,000 gamma-ray simulation on the Moon surface is shown in Fig. 12. The mean energy deposit of a 10 GeV gamma-ray in the total scintillating volume is about 357 MeV. The energy distribution pattern is well described by a Gamma distribution and could also be used for photon or electron-positron identification and hadron rejection (Wigmans and Zeyrek 2002). In fact, the showers initiated by the gammas are shifted to larger depths inside the absorber compared to those of electrons. Furthermore, fluctuations in the amount of energy deposited in a given slab of material are larger for showers induced by photons than for showers induced by both electrons and positrons. However, to obtain a reliable estimated energy and particle selection, a systematic study of the Mooncal response and its slabs inter calibration is necessary (Wigmans and Zeyrek 2002). Finally, it is worthy to remark that at present the Mooncal angular resolution is still under study: however preliminary results suggest this resolution to be comparable (or better) with the one obtained by imaging Cerenkov telescope (∼0.1–0.5 degrees).

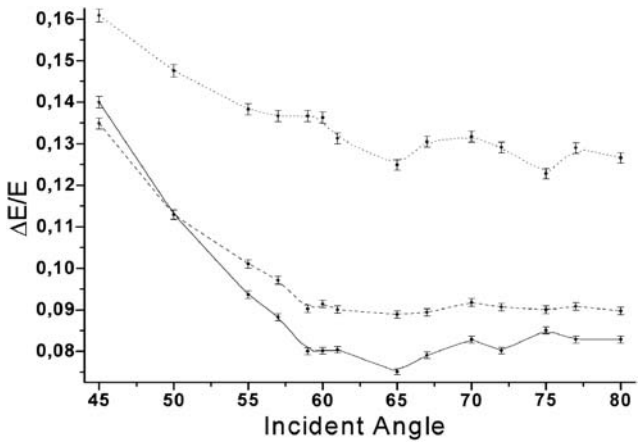


**Fig. 10** Energy resolution versus the incidence angles for the parameters $r = 0.5$ cm, $L = 150$ cm and $d = 4$ cm, the different energies of incident photons are 5 GeV (*dotted line*), 20 GeV (*dashed line*) and 50 GeV (*continuous line*)

## 6 Conclusions

This preliminary study discusses the usage of lunar regolith as a radiator of a large acceptance gamma-ray calorimeter

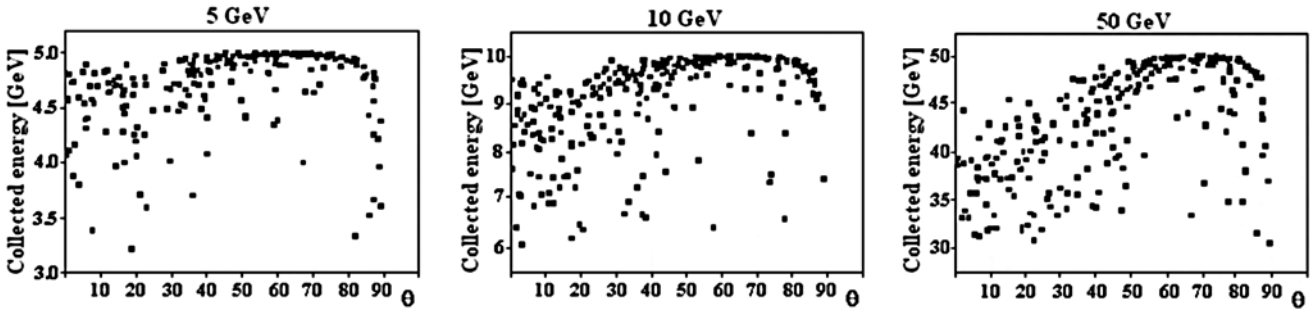


**Fig. 11** Energy was collected with $E > 0.6E_o$ for $E_o = 5$, 10 and 50 GeV gamma-rays as a function of incident angle. The Mooncal parameters are $r = 0.5$ cm, $L = 150$ cm and $d = 4$ cm

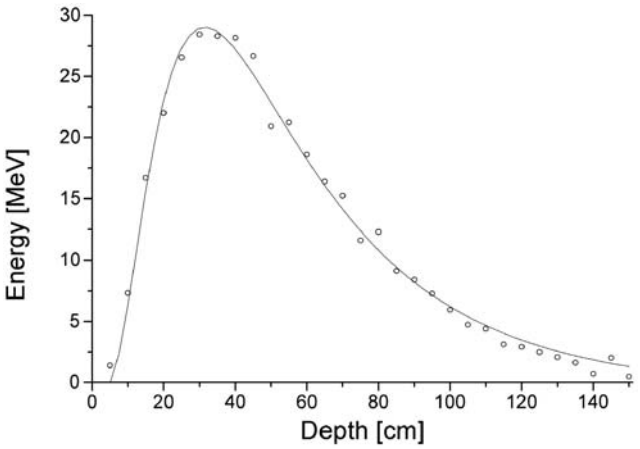


**Fig. 12** Energy deposits on 5 cm slabs of scintillating bars produced by 10 GeV incident gamma-rays on the calorimeter with parameters $r = 0.5$ cm, $L = 150$ cm and $d = 4$ cm

detector which could be part of the scientific program on our satellite. This design reduces by two orders of magnitude both the cargo volume and transport weight, allowing for an optimised number of missions needed to build the lunar calorimeter.

The energy interval covered by the proposed regolith-scintillator calorimeter (10 GeV–few TeV) is of great scientific interest for the study of high energy gamma-rays originating from point-like or diffused sources.

Monte Carlo simulations of the instrument were performed to determine both the energy resolution response as a function of the design parameters. The results of the simulations suggest that the asymptotic energy resolution can be better than 8% for a realistic configuration.

**Acknowledgement** We would like to thank A. Oliva for his valuable observations. ASI grants for contract INAF-LUNA-PMG-RP.

## References

Achenbach, P. et al.: In-beam tests of scintillating fibre detectors at MAMI and at GSI. arXiv:0802.2830v1 [nucl-ex], 20 Feb (2008)

Agostinelli, S., et al.: GEANT4—a simulation toolkit. Nucl. Inst. Methods Phys. Res. A **506**, 250 (2003)

Aharonian, F.A., et al. (H.E.S.S. Collaboration): Energy dependent gamma-ray morphology in the pulsar wind nebula HESS J1825-137. Astron. Astrophys. **460**, 365 (2006)

Aharonian, F.A., et al. (H.E.S.S. Collaboration): Detection of extended very-high-energy gamma-ray emission towards the young stellar cluster Westerlund 2. Astron. Astrophys. **467**, 1075 (2007)

Aharonian, F.A., et al. (H.E.S.S. Collaboration): Discovery of very high gamma-ray emission coincident with molecular clouds in the W 28 (G6.4-0.1) field. Astron. Astrophys. **481**, 401 (2008a)

Aharonian, F.A., et al. (H.E.S.S. Collaboration): Upper limits from HESS active galactic nuclei observations in 2005–2007. Astron. Astrophys. **478**, 387 (2008b)

Aharonian, F.A., et al. (H.E.S.S. Collaboration): HESS very-high-energy gamma-ray sources without identified counterpart. Astron. Astrophys. **477**, 353 (2008c)

Beilick, M.: HESS observations of extragalactic objects. Astrophys. Space Sci. **309**, 139 (2007)

Bertone, G., Hooper, D., Silk, J.: Particle dark matter: evidence, candidates and constraints. Phys. Rep. **405**, 279 (2005)

Champbell, B.A.: Comment on "Regolith layer thickness mapping of the Moon by radar and optical data. Icarus **158**, 560 (2002)

De Salvo, R.: Fiber/scintillating fiber ("Spaghetti") calorimetry. Nucl. Phys. B **44**, 122 (1995) (Proc. Suppl.)

Dinu, N., Battiston, R., Boscardin, M., et al.: Development of the first prototypes of silicon photomultiplier (SiPM) at ITC-irst. Nucl. Instrum. Methods Phys. Res. A **572**, 422 (2007)

Dubus, G.: High energy gamma-ray emission from binaries. New Astron. Rev. **51**, 778 (2008)

Fan, Y.-Z., Piran, T.: High energy gamma-ray emission from gamma-ray bursts—before GLAST. arXiv:0805.2221v3, 4 Jun (2008)

Foing, B.H.: The Moon as a platform for astronomy and space science. Adv. Space Res. **18**(11), 17 (1996)

Funk, S.: Status of identification of VHE gamma-ray sources. Astrophys. Space Sci. **309**, 11 (2007)

Funk, S.: VHE Gamma-ray supernova remnants. Adv. Space Res. **41**, 464 (2008)

Gavler, S.B., Carlson, P., Conrad, J.: Fluctuation studies and energy reconstruction in a segmented calorimeter. In: IEEE Nuclear Science Symposium Conference Record, N10-5, p. 177 (2006)

Greiner, I.: The galactic Gamma-Ray Club. In: 30th ICRC (2007)

Griffin, M.D.: The text of Griffin's remarks on 1 November 2005 can be found at http://www.nasa.gov/pdf/137173main_mg_csis.pdf

Heiken, G.H., Vaniman, D.T., French, B.M.: Lunar Source Book, a User's Guide to the Moon. Cambridge University Press, Cambridge (1991)

Hinton, J., Egberts, K., for the HESS Collaboration: High energy stereoscopic system: Latest results. Adv. Space Res. **41**, 477 (2008)

King, E.A.: The lunar regolith: physical characteristics and dynamics. Philos. Trans. R. Soc. Lond. A **285**, 273 (1977)

Kobayashi, T., Komori, Y., Yoshida, K., Nishimura, J.: The most likely sources of high-energy cosmic-ray electrons in supernova remnants. Astrophys. J. **601**, 340 (2004)

Komle, N.I., Kaufmann, E., Kargl, G., Gao, Y., Rui, X.: Development of thermal sensors and drilling systems for lunar and planetary regoliths. Adv. Space Res. **42**, 363 (2008)

Kuhlen, M., Diemand, J., Madau, P.: The dark matter annihilation signal from galactic substructure: predictions for GLAST. arXiv:0805.4416v1, 29 May (2008)

Moiseev, A.A.: Gamma-ray Large Area Space Telescope: Mission overview. Nuc. Instrum. Methods Phys. Res. A **588**, 41 (2008)

Pavlidou, V., Siegal-Gaskins, J.M., Fields, B.D., Olinto, A.V., Brown, C.: Unresolved unidentified source contribution to the Gamma-ray background. Astrophys. J. **667**, 27 (2008)

Perrin, D., Sonderegger, P.: Electromagnetic calorimeter with scintillating optical fibers. CERN-OM-SPS/81-7 (1981)

Shkuratov, Y.G., Bondarnko, N.V.: Regolith layer thickness mapping of the Moon by radar and optical data. Icarus **149**, 329 (2001)

Shkuratov, Y.G., Bondarnko, N.V.: Reply to the comment. Icarus **158**, 562 (2002)

Spudis, P.D.: The case for renewed human exploration of the Moon. Earth Moon, Planets **87**, 159 (2001)

Strong, A.W.: Source population synthesis and the Galactic diffuse gamma-ray emission. Astrophys. Space Sci. **309**, 35 (2007)

Tajima, H.: GLAST tracker. Nucl. Instrum. Methods Phys. Res. A **569**, 140 (2006)

Wigmans, R., Zeyrek, M.T.: On the differences between calorimetric detection of electrons and photons. Nucl. Instrum. Methods Phys. Res. A **435**, 385 (2002)

Wilkinson, A., DeGennaro, A.: Digging and pushing lunar regolith: Classical soil mechanics and the forces needed for excavation and traction. J. Terramechs. **44**, 133 (2007)